Available online at www.sciencedirect.com
ScienceDirect
Carbohydrate Research 341 (2006) 2521–2530
Carbohydrate RESEARCH

Swelling behavior of the cellulose Iβ crystal models by molecular dynamics

Toshifumi Yui,* Shinya Nishimura, Shingo Akiba and Sachio Hayashi

Department of Applied Chemistry, Faculty of Engineering, Miyazaki University, Miyazaki 889-2192, Japan

Received 14 July 2005; received in revised form 7 April 2006; accepted 7 April 2006
Available online 17 August 2006

Abstract—The various crystal models of cellulose Iβ, each differing in crystal size, have been studied by computer simulation using the AMBER molecular-dynamics package and the GLYCAM parameters. The four types of crystal model were constructed by a combination of two base-plane sizes, consisting of either 24 or 48 chains and two chain lengths having either 10 or 20 residues. The base planes of the crystal models were composed by the edges of the [1, 1, 0], [1, −1, 0], and [1, 0, 0] crystal planes, where the [1, 1, 0] plane was assigned to the longest edge. The crystal models were soaked in water boxes to investigate their swelling behavior. Unexpectedly, the crystal models twisted quickly to form a slightly right-handed shape during the initial ~50 ps and that, in a steady, swollen state, the twisted forms remained for the rest of the simulation time. In spite of such overall deformation, the inner part of the swollen model fairly reproduced the important structural features of the original crystal structure, such as the rotational positions of the substituent groups and the hydrogen-bonding scheme. On heating the crystal model up to 550 K, the twisted shape was conserved in most of the temperature range, while the initial conformations of the substituent groups deviated above ~430 K, followed by appreciable disordering in chain sheets at higher temperatures. It is suggested that some internal tensions are involved within a chain sheet of the initial structure. In the course of swelling, some of these tensions were released to introduce a twisted shape in the crystal models.

Keywords: Cellulose Iβ microfibrils; Crystal model; Molecular dynamics

1. Introduction

A highly crystalline microfibril of cellulose is found among all higher plants, and some fungi, algae, and bacteria, either as a cell-wall material or an extracellular product. The uniaxially oriented cellulose microfibrils, therefore, can serve for X-ray diffraction measurements. Following the historical study reported by Meyer and Misch,[1] several attempts to determine the native cellulose crystal structure, earlier termed cellulose I, in atomic detail were made by X-ray diffraction analysis combined with computational modeling.[2–4] It was also known that the diffraction patterns of native cellulose microfibrils are diverse depending on the source. High resolution solid-state ^{13}C NMR measurements allowed clear interpretation of these crystalline diversities; native cellulose crystals consist of the two crystalline forms, designated as Iα and Iβ, and their relative amounts depend on the cellulose origin.[5,6] The diffraction data were convoluted into the one-chain triclinic unit cell and the two-chain monoclinic unit cell, corresponding to the Iα and Iβ phases, respectively, by using electron microdiffraction analysis.[7–9] These studies revealed that the single-chain unit cell of cellulose Iα was doubled to form the two chain, cellulose Iβ unit cell by sliding chain sheets along their axes. The two chains of the latter unit

Abbreviations: AMBER, assisted model building and energy refinement; CHARM, chemistry at Harvard macromolecular mechanics; ESP, electrostatic potential; GLYCAM, glycosides and glycoproteins with AMBER; RESP, restricted electrostatic potential; RMSd, root-mean-square difference; MM3, molecular mechanics 3; VMD, visual molecular dynamics.

* Corresponding author. Fax: +81 985 58 7323; e-mail: tyui@cc.miyazaki-u.ac.jp

0008-6215/$ - see front matter © 2006 Elsevier Ltd. All rights reserved.
doi:10.1016/j.carres.2006.04.051

cell were crystallographically independent and were classified into either an origin chain or a center chain, depending on a location on the base plane. With the knowledge of the two crystalline phases for the native cellulose microfibrils, the published X-ray diffraction data of algae cellulose were reanalyzed to establish the cellulose Iβ structure.[10] The crystal structure of cellulose Iα has been subjected to pure computational modeling searches against the observed unit-cell parameters.[11–14] Recently, Nishiyama et al. conducted landmark work of the cellulose crystal structures, where synchrotron X-ray and neutron fiber-diffraction measurements were carried out for both the cellulose Iα[15] and Iβ[16] microfibrils. In particular, by comparing the fiber diagrams of normal hydrogenated and deuterated samples, the neutron-diffraction method allowed them to determine the orientations of the hydroxyl groups, giving a concrete scheme of hydrogen-bonding networks.

In addition to the various physical and chemical analyses, including the diffraction measurements, the cellulose crystals have been subject to molecular dynamics (MD) studies in order to reveal the crystal conversion,[17] the structural details,[18–21] the physical or mechanical properties,[22–27] and the interface behaviors with the aqueous phase of pure water[18–21] or of solutions that include small molecules.[28,29] In these studies, the periodic boxes were set to establish infinite crystalline and aqueous phases with either the NTV or NTP conditions. In contrast to water molecules, which are able to move about freely between the neighboring periodic boxes, the cellulose chains, ranging from 4 to 6 repeating units, are covalently connected to those in the adjacent boxes. It, however, may have been possible that a surface disorder or crystal conversion had taken place, with motions of a magnitude near to or larger than the box size. In contrast to the infinite systems, the finite, small-crystal models of native cellulose involving about 40 glucose residues were examined by MM3 minimizing.[11–13] Despite the limited size of the crystal models, the optimized structures fairly reproduced the hydrogen-bond geometries and provided reasonable predictions of thermodynamics values. Recently, a dynamics study of the solvated molecular assembly consisting of five cellulosic chains with DP = 30 was reported.[30] It was observed that the chains were loosely aggregated without the distinct formation of an inter-chain hydrogen bond. The present report thus attempts to observe dynamic behavior of finite but possibly the largest crystal models ever studied for a solvation system, and expects to provide a new understanding as regards chain motions on the crystal surfaces or edges, or, possibly, those in overall crystals. In addition, we have been also motivated by Nishiyama's achievement of the neutron diffraction study,[16] since their work allowed us to construct the crystal models with an unambiguous hydrogen-bonding scheme.

2. Methods

2.1. Construction of crystal models

Figure 1 shows the atom labeling and the torsion-angle parameters of primary interest in defining the cellulose conformation. The Ω angle represents the orientation of the hydroxymethyl group and their representative conformers are designated either as *gg*, *gt*, or *tg* as depicted in Figure 2.

The atomic coordinates, including hydroxyl-group orientations, and lattice parameters, for cellulose Iβ used in the present calculations were obtained from the results of the fiber-diffraction study reported by Nishiyama et al.[16] The cellooligosaccharides consisting of either 10 or 20 glucose units were spatially arranged according to the crystal symmetry to construct the crystal models with various dimensions. The torsional positions of hydroxyl groups were those designated as the **A** type of Nishiyama's model,[16] which involved the intensive inter-chain hydrogen bonds of O6D–O3 within both the origin- and center-chain sheets, while the latter sheet comprised an additional, weak bond between O6D–O2.[16] Table 1 describes the compounds of the four crystal models examined in the present study and their solvation systems; the dimensions of the crystal models, the periodic box types, and the number of cellulose chains and water molecules involved. Figure 3 depicts the base plane projections of the largest crystal model (**D**) among the four models. The base plane comprises the $[1,1,0]$ and $[1,-1,0]$ crystal planes where the former corresponds to the longest edge. The $[1,0,0]$ plane of a single chain constitutes the corners of the base plane. The chain sheets align diagonally along the $[1,0,0]$ and $[2,0,0]$ planes consisting of the origin- and center-chain sheets, respectively. As defined in Table 1, the four models differ in the number of chains involved in each edge or a chain length, while all the base planes are of the

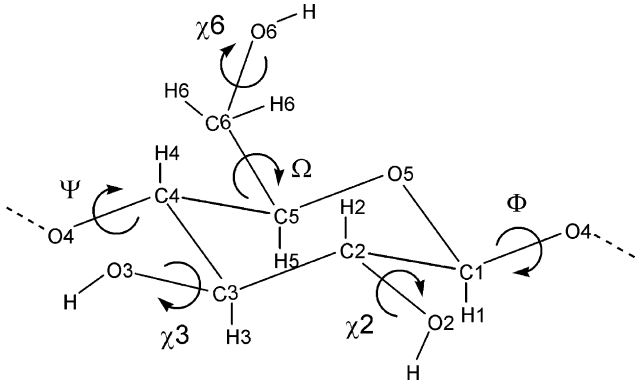

Figure 1. Atomic labeling and torsion-angle parameters of primary interest. The torsion angles are defined by atom sequence of Φ = H1–C1–O4–C4, Ψ = C1–O4–C4–H4, Ω = O5–C5–C6–O6, χn = Hn–Cn–On–H ($n = 2,3$), and $\chi 6$ = C5–C6–O6–H.

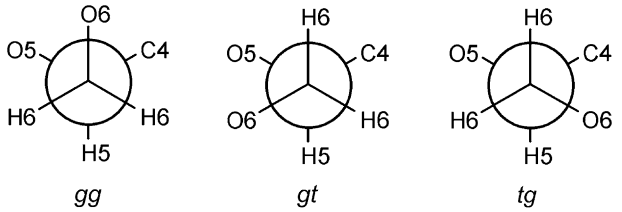

Figure 2. Projections of the three representative conformers of a hydroxymethyl group.

of deviation from the initial planar structure is defined by the torsion angles that consist of the virtual bonds connecting the center of gravity of a certain specified residue(s). As discussed below, since a twisted motion took place over the chain-sheet plane during swelling dynamics, the amount of deviation is described by the multiple torsion angles, labeled by a sheet-twisting angle, Θ, along the chain axis. The angles defining the

Table 1. Crystal model and periodic box systems calculated in the present study

Label	Base-plane dimensions[a]	Periodic box type[b]	DP	No. of molecules	
	No. of chains [lattice plane]× ...			Residue	Waters
A	6[1,1,0]× 1[1,0,0]× 4[1,−1,0]	Oct	10	240	8459
B	6[1,1,0]× 1[1,0,0]× 4[1,−1,0]	Rec	20	480	11,257
C	8[1,1,0]× 1[1,0,0]× 6[1,−1,0]	Oct	10	480	12,980
D	8[1,1,0]× 1[1,0,0]× 6[1,−1,0]	Rec	20	960	24,196

[a] The edge faces consisting of a crystal model. The edges listed are the minimum set to describe the base-plane dimensions of each crystal model.
[b] Rec: rectangular box; Oct: octahedral box.

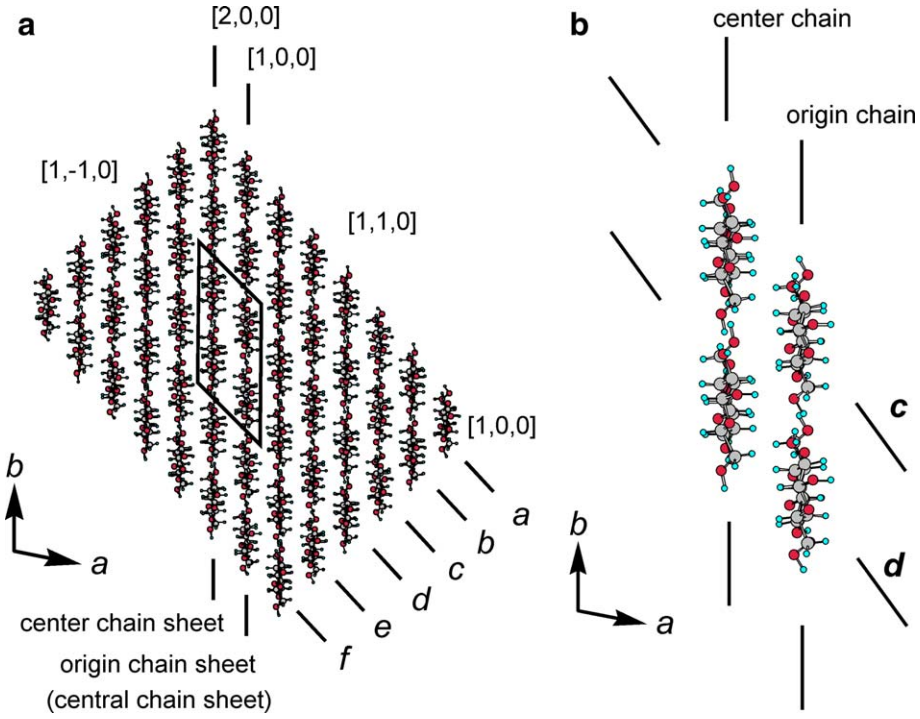

Figure 3. Projections of the *ab* base plane of the **D** model (a). The crystal planes constituting the base-plane edges and the labels of the chain positions are indicated. A parallelogram defines the core unit, of which an enlarged scheme is shown at the right (b).

same ratio. Figure 3 also defines the 'core' unit, which involves the four chains residing inmost in the crystal model, and the base-plane location (*a–f*) along the $[1,-1,0]$ edge. The residues in the core unit are considered to be placed within the environment proximate to the actual crystal. The origin-chain sheet passing through the core unit is shown in Figure 4, where each residue is numbered along the helix axis. The amount

deviation between both terminal ends are designated either as Θ_{+10} or Θ_{-10}, depending on the direction of a virtual-bond sequence, for the second terminal ends, Θ_{+9} or Θ_{-9}, and so on. A chain sheet of complete a plannar structure is defined by 0° for all the Θ angles, and when twisting into a clockwise direction, the Θ is positive. Obviously, the largest deviation of the angle occurs at the terminal ends or next to the ends.

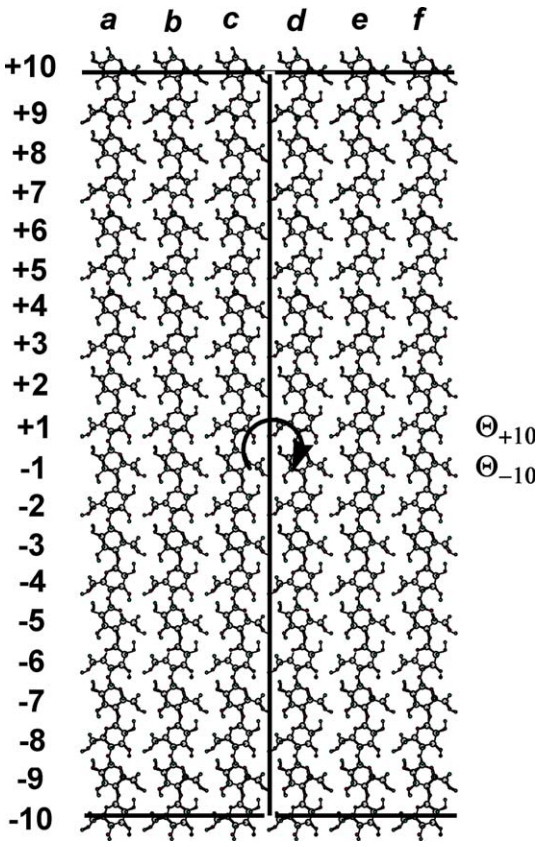

Figure 4. A central origin-chain sheet along with residue positional labeling. Sheet-twisting torsion angles are defined by the virtual bonds connecting the centers of gravity (**G**) of residue(s); $\Theta_{+10} = \mathbf{G}(a/+10) - \mathbf{G}(c/+10, d/+10) - \mathbf{G}(c/-10, d/-10) - \mathbf{G}(f/-10)$, $\Theta_{-10} = \mathbf{G}(a/-10) - \mathbf{G}(c/-10, d/-10) - \mathbf{G}(c/+10, d/+10) - \mathbf{G}(f/+10)$, and so on.

2.2. Molecular dynamics calculation

All MD simulations were performed with the SANDER module of the AMBER 8 package[31] along with the GLYCAM 04 carbohydrate parameter set and RESP atomic charges.[32–34] The crystal models were soaked in the periodic box of either the rectangular or octahedral box with buffer sizes of 10 or 14 Å. The boxes were filled with TIP3P[35] water molecules. The initial positions of water molecules were optimized by 500 cycles of steepest descent energy minimization, followed by 1500 cycles of conjugated gradient minimization, while the structures of the crystal models were fixed with the constrained force of 500 kcal/mol Å^2. The whole systems were then subjected to a combination of 1000 cycles of steepest descent and 4000 cycles of conjugated gradient energy minimizations. In the subsequent dynamics calculations, Newton's equations of motion were integrated by using a Verlet algorithm with a 2 fs time-step.[36] Initial atomic velocities were assigned from a Maxwellian distribution at 20 K. A constant temperature of 300 K was maintained through coupling to the external bath with a coupling constant of 0.2 ps. After an initial 100 ps run of constant-volume dynamics, the simulations were then switched to constant pressure dynamics at 1 bar with isotropic position scaling and a pressure relaxation time of 2.0 ps. As with the minimization step, a subsequent 500 ps run was carried out under the fixed crystal structures with the constrained force of 10 kcal/mol Å^2. Finally, under the NTP condition, a swelling simulation of crystal models without any constraint was implemented for 1 or 2 ns. All minimizations and dynamics were performed with a dielectric constant of unity and a cut-off value for non-bonded pair interactions of 10.0 Å. Throughout dynamics calculations, the SHAKE option[37] was adopted for bond interactions involving hydrogen atoms and the Particle Mesh Ewald method[38] was applied for calculations of long-range, non-bonded interactions.

The dynamics with a controlled heating rate was performed for the **D** crystal model under similar conditions, with the foregoing dynamics except for the following scheme. After the equilibration run with constrained solute motions, the non-constrained, swelling run under the constant temperature of 300 K was carried out for 500 ps. The dynamics was subsequently switched to the heating run for 1 ns where the temperature of the external bath was gradually increased at a constant heating rate of 0.25 K/ps, until reaching the final temperature of 550 K.

VMD 1.8.3 was used for molecular visualization and for animating trajectory data.[39]

3. Results and discussion

3.1. Swelling behavior and features of swollen structures

The RMSd trajectories of the four crystal models are compared in Figure 5. When visually inspecting the dynamics structure using the molecular dynamics viewer, it was observed in the early stage of dynamics, during an initial 50 ps that the overall shapes of all the crystal models were twisted in a clockwise direction along the fiber axis. The twisted structures were then maintained for the rest of the dynamics time accompanied by more distinct, local motions, especially around the edges of the crystal models. The variations of RMSd values in Figure 5 obviously reflect such a twisting motion. At the steady state, larger deformations were observed in the longer models with 20-residue chains, **B** and **D**, than the respective 10-residue chain models, **A** and **C**, due to the larger amplitude motions involved in the terminal ends of the 20-residue chain sheets. On the other hand, the model **C** exhibited the smallest RMSd values among the four trajectories throughout the simulation time, and a 48-chain model, **D**, gave smaller RMSd values than its 24-chain counterpart, the model **B**. This suggested that lateral expansions in the base-plane dimensions of the

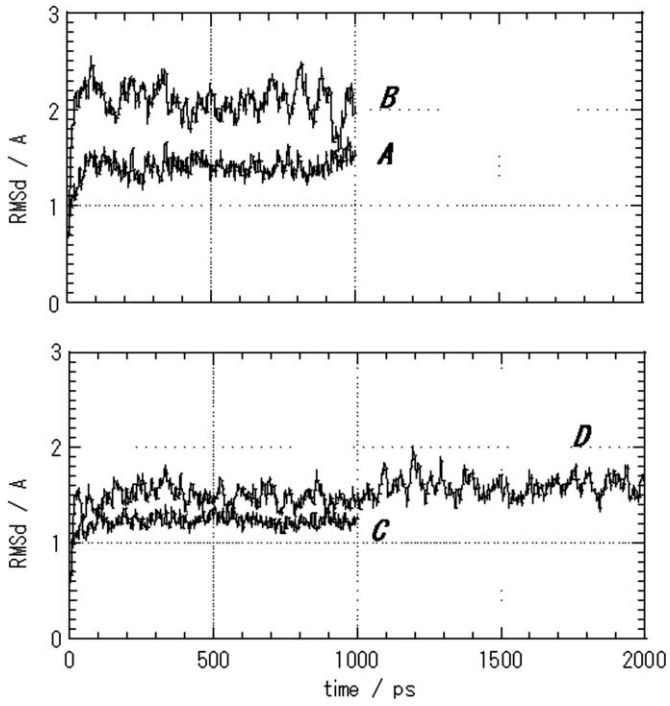

Figure 5. RMSd trajectories calculated for the four crystal models.

crystal model suppressed deviations. It should be noted that the RMSd trajectories of the central chain sheets consisting of the origin chains showed essentially similar behavior to those given in Figure 5. This obviously indicated that twisting motions of individual chain sheets reflected deformation of the overall crystal model. Figure 6 compares variations of a sheet-twisting torsion angle, Θ, evaluated from the central origin-chain sheet with respect to the residue number. The Θ values in Figure 6 are those averaged between a positive and negative angle numbers, and over the trajectories from 500 ps to 1 ns. As indicated by the positive values of Θ, chain sheets are twisted clockwise in all four crystal models. In comparison with the results given in Figure 5, the values of the twisting angles at the terminal ends are of the same order as those of the RMSd among the four crystal models. While the $\Theta_{\pm 10}$ of the model **B** is largest among the four terminal angles, the model **D** gives the smallest value. Both $\Theta_{\pm 5}$ of the models **A** and **C** appears between the foregoing angles. When comparing the models having the same base plane, the Θ values observed for the 20-residue models increase more gently than those of their 10-residue counterparts. As a result, at the same residue position, the Θ values of the **D**, **C**, **B**, and **A** models appear with an increasing order. A chain sheet tends to deviate less while increasing longitudinally as well as laterally.

The structural features of the **D** model, the largest system herein, were further investigated by averaging the trajectories over the final 1 ns of the 2 ns unconstrained dynamics. Figure 7 shows the averaged values of Ω and their RMSd of the residues consisting of the base planes at the middle layers. The observed Ω angles for Nishiyama's crystal structure were 169°. for the origin chain and 158°. for the center chain, both corresponding to the *tg* conformation.[16] In spite of a twisted deformation of the model, the averaged conformations in the swollen structure are near *tg*, except for those located in the surface residues. One residue belonging to the inner part of the -1 layer exhibits only a deviated *gg* conformation. The averaged Ω values of 48 surface residues shown in Figure 7 are classified into *gt* for 21 residues, *gg* for four, and *tg* for 12. The averaged values of the remaining 11 residues, accompanied by large RMSds, indicate multiple conformations that took place in the course of the final 1 ns. The population ranking of the hydroxymethyl-group orientation observed for an isolated glucopyranose in both solid and solution states is suggested to be in the order *gt*, *gg*, and *tg*.[40–43] As for the surface residues in the present crystal model, it should be noted that the 12 *tg* conformations arose in the hydroxymethyl groups that were oriented inside. The surface residues on the $[1,-1,0]$ planes tended to involve larger RMSd values, where some indicated multiple conformations. In addition, the hydroxyl groups of the surface residues also exhibited multiple conformations as a result of interaction with the surrounding solvent water molecules. Similar swelling behavior was observed in the remaining residue-layers of the base plane, except for those terminal layers (± 10 and, probably, ± 9) of the crystal model, which comprised more-disordered rotation patterns. Therefore, water molecules seemed

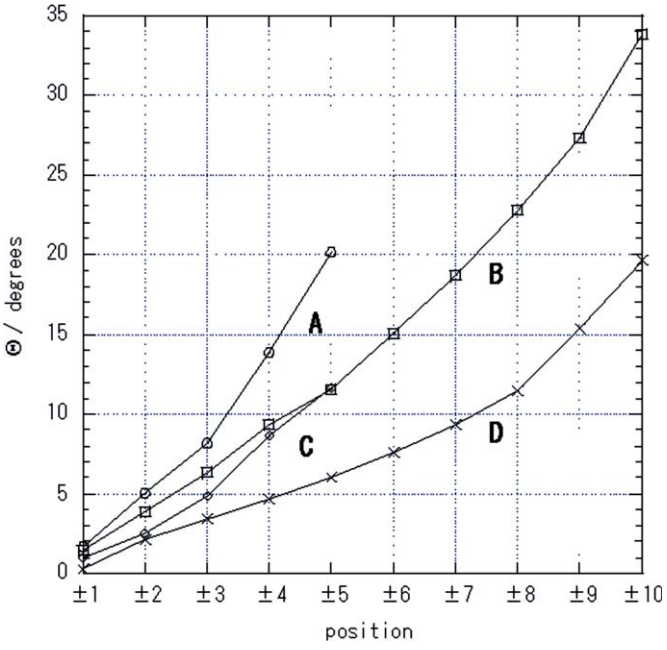

Figure 6. Variations of sheet-twisting torsion angles, Θ, with respect to chain position. The Θ values are averaged from 500 ps to 1 ns trajectories of the four crystal models.

a

31(53)	58(12)	52(15)	58(12)	53(14)	68(30)	54(14)	60(14)
60(22)	176(13)	166(8)	179(13)	165(9)	179(15)	163(9)	137(52)
39(34)	161(9)	179(12)	162(9)	180(11)	163(8)	179(12)	163(8)
61(25)	177(12)	162(8)	179(11)	162(8)	178(12)	162(8)	176(12)
46(54)	164(8)	-179(10)	163(8)	178 (14)	163(8)	176(12)	165(8)
32(59)	-51(11)	163(9)	176(13)	161(17)	-128(65)	165(8)	-56(13)

b

-59(12)	162(9)	-64(34)	163(8)	-153(56)	163(9)	176(13)	69(36)
148(37)	178(11)	163(8)	178(12)	-145(4)	178(12)	163(8)	13(54)
39(34)	162(8)	178(12)	162(11)	180(11)	163(8)	179(12)	57(13)
162(9)	-177(30)	163(8)	178(12)	163(8)	179(12)	162(8)	14(51)
-91(66)	165(8)	-179(13)	164(9)	178(12)	164(9)	-37(27)	42(38)
67(50)	55(14)	60(12)	53(20)	59(13)	54(16)	62(11)	51(23)

[1,-1,0]

[1,1,0]

Figure 7. The averaged Ω and their RMSd values in a parenthesis calculated from the final 1 ns trajectories of the **D** model. The values are placed such as to represent the actual chain positions on the base plane layers of -1 (a) and $+1$ (b), where a shaded rectangle indicates the position for a center chain.

to interact mostly with the residues belonging to the surface layers at each crystal face and rarely penetrated into the second layers. When evaluating the averaged number of accessible waters to the surface residues in Figure 7, the residues at the $[1,0,0]$ corners were most exposed to solvent waters, giving the number of accessible waters of about 12, followed by those at the two other corners, of about 11. The surface residues on the $[1,1,0]$ and $[1,-1,0]$ planes were found to involve smaller number of accessible waters, ranging about 6 to 7.

Table 2 lists the hydrogen-bond geometries detected in the core unit of the swollen structure. The core unit well reproduced the hydrogen-bonding scheme proposed for the original crystal structure, including the bonding directions. The hydroxyl group conformations in the core unit were also found near the crystal struc-

Table 2. Averaged geometries of hydrogen bonds in the core unit of **D** model

Bond type				Distance[a] (RMSd) (Å)	Occupancy[b] (%)
Atom	Chain/residue no.	Atom	Chain/residue no.		
Intra-chain bonds in origin chain					
O-6	*c*/−1	H–O2	*c*/+1	2.835(0.14)	99.90
	d/−1		*d*/+1	2.815(0.13)	100.00
Observed				2.765	
O-5	*c*/+1	H-O3	*c*/−1	2.754(0.10)	99.10
	d/+1		*d*/−1	2.759(0.09)	99.20
Observed				2.764	
O-4	*c*/−1	H-O2	*c*/+1	2.718(0.00)	0.10
Observed				2.797	
Intra-chain bonds in center chain					
O-6	*c*/−1	H-O2	*c*/+1	2.718(0.09)	100.00
	d/−1		*d*/+1	2.737(0.11)	100.00
Observed				2.865	
O-5	*c*/+1	H-O3	*c*/−1	2.718(0.09)	100.00
	d/+1		*d*/−1	2.722(0.09)	99.90
Observed				2.705	
O-4	*c*/−1	H-O2	*c*/+1	2.772(0.70)	0.70
Observed				None	
Inter-chain bonds in origin chain					
O-3	*d*/+1	H-O6	*c*/+1	2.763(0.10)	99.90
	c/−1		*d*/−1	2.765(0.10)	99.90
Observed				2.892	
O-2	*d*/+1	H-O6	*c*/+1	3.336(0.13)	38.30
	c/−1		*d*/−1	3.343(0.12)	36.60
Observed				None	
Inter-chain bonds in center chain					
O-3	*c*/−1	H-O6	*d*/−1	2.891(0.12)	99.80
	d/+1		*c*/+1	2.891(0.12)	99.60
Observed				2.711	
O-2	*c*/−1	H-O6	*d*/−1	3.347(0.11)	40.20
	d/+1		*c*/+1	3.350(0.12)	35.70
Observed				3.211	

[a] Distance between oxygen atoms.
[b] Time percentage that hydrogen bond forms the geometry defined by the cut-off distance of 3.5 Å and the angle cut-off 120°.

ture, but their rotational motions made the O6–H–O2 intermolecular bonds a minor interaction, with occupancy of about 40% and the O2–H–O4 intra-molecular bonds, a negligible one. Since the core unit represented the rest of the inner residues of the crystal model, the swollen structures well established the fundamental features of the original cellulose Iβ crystal, in spite of their twisted forms.

Our primary concern, therefore, is whether the swelling behavior and structural features observed by the present dynamics can be applicable to those of the actual microfibrils in an aqueous environment. In terms of the base-plane dimensions, the **D** crystal model with edges of about 2×4 nm reaches the comparable sizes of the wood microfibrils,[44] whereas its longitudinal length is too small to be called a 'fibril'. Considering significant deviations derived from the present crystal models, it is, however, possible that a twisted feature can be present in a perfect microfibril of infinite length under certain conditions. This results in the helical propagation of a microfibril during its biosynthesis. As another probable prediction, the present dynamics behavior could also be applicable to describe a local swelling event occurring at the surface or terminus of a real microfibril. The resulting deformed portions may serve as the target for some enzymes or binding proteins.

3.2. Heating dynamics

Another striking result obtained from the present simulation study was that a chain apparently exhibited spontaneous motion; it was quickly initiated after releasing the constraints imposed on the chains at 300 K and arose almost uniformly over the chain sheets, including the largest, central chain sheet. It seemed that the chain sheets had established an internal strain upon crystallization of a microfibril through biosynthesis. Some possible candidates would be listed as a source of the strain. The strict twofold conformation of the cellulose chain can exist only in the crystalline environment where the lattice force is exerted on the chain. In an isolated state, the twofold helix is relaxed into slightly deviated

conformations. The *tg* orientation of hydroxymethyl groups, being unfavorable for a glucose residue, is one of the representative features for the native cellulose crystals, as well as the parallel chain arrangement. It should be noted that all the O6–H groups participate in both the intra- and inter-molecular hydrogen bonds. The strain originating from the unfavorable orientation of the substituent groups may cooperatively expand over the chain sheet through hydrogen bonds, which can be enhanced by the parallel arrangement of chains. Minimizing the **D** model in vacuum conditions, introduced a slight deviation of the central chain sheet, giving $\Theta_{\pm 10} = 3.2°$. Additional internal motions would be required as a kinetic factor for chain sheets to be deviated with larger angles. A solvent effect could have been one among the possible causes of a crystal deformation in terms of both thermodynamics and kinetics, but is not a primary one. If it had been so, a deviation should have taken place gradually at the edges of a chain sheet.

In order to examine the internal tension involved in the initial crystal model, partly expecting to observe the crystal-phase transition, a heating dynamics of the **D** model was performed with a constant heating rate of 0.25 K/ps. Figure 8 shows the two trajectories of RMSd values, each differing in the reference coordinate adopted. The RMSd2 curve, referring to the final twisted structure under constant temperature dynamics, exhibit smaller changes than the RMSd1 curve based on the starting crystal structure. It was revealed by visual inspection that the crystal model continued to display a twisted shape, even in the elevated temperatures. Both the RMSd curves increased steeply over the range from 400 to 430 K, followed by a steady state for a next 100 ps, where the Ω and χ angles of the substituent groups in the core unit started to rotate into different conformations from those of the original crystal structures. Intermolecular hydrogen bonds still existed over the temperature range, while developing a different scheme in addition to the original one. No significant variation was observed in the Θ angles of the central chain sheet during most of the heating time. In Figure 8, as temperature reached to about 480 K, the RMSd2 curve again began to rise, whereas the RMSd1 plot stayed at almost constant values, a behavior indicating that the twisted feature has gradually dissipated in this temperature range. Thus, the trajectories of the present heating dynamics indicate that, even expanding the crystal dimensions due to heating, the twisting structure was derived from the original hydrogen-bonding scheme.

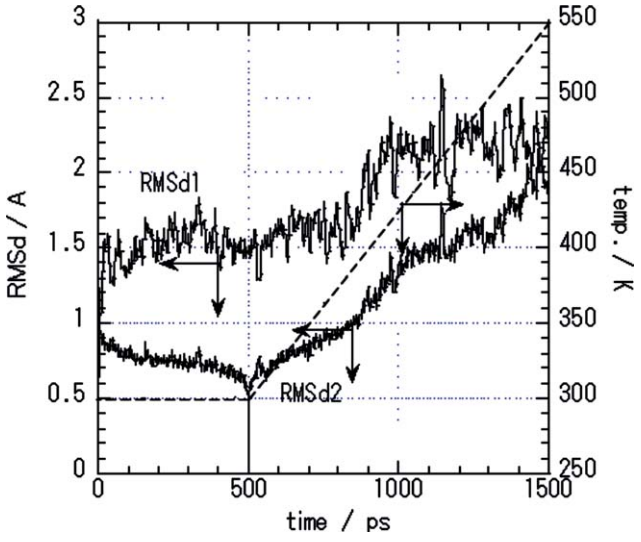

Figure 8. RMSd trajectories obtained from the heating dynamics of the **D** model. The RMSd are calculated with respect to the starting structure at 0 ps (RMSd1) and the final coordinates of the constant temperature dynamics at 500 ps (RMSd2). Temperature variations are shown by a broken line.

4. Conclusions

The present dynamics study of the cellulose crystal models unexpectedly proposed their twisting deformation when swelling in aqueous environment. Matthews et al. also reported twisting behaviors of cellulose crystal models in their similar molecular-dynamics study using the CHARM force field.[45] Some representative features of the original crystal structure, such as the rotational positions of the substituent groups and the hydrogen-bonding scheme, are well conserved in the swollen structures. It was also found that apparent overall shape of the twisted crystal model originated from the right-handed twisting motions occurring at individual chain sheets. Therefore, a possible cause for such a transformation would be an inherent tension probably involved in both the origin- and center-chain sheets. It is unlikely that solvent waters play a primary role in the twisting motion, considering instead a spontaneous deformation of individual chain sheets. Whereas random motions of surrounding water molecules may have triggered off a twisting motion, such an effect of solvent waters is rather restricted to the surface of the crystal models, and not affecting the overall shape.

It should be also pointed out that the crystal models continuously exhibited their twisted forms from an early stage of simulation. In the **D** model, the constant, twisted structure was observed for next 2 ns, and even at elevated temperature, up to about 430 K. With a more prolonged simulation at the higher temperature, one would observe a structure transition to a different crystal phase. Prior to the present study, we performed similar dynamics calculations for the models of cellulose Iβ, using the GLYCAM 2000 parameter set with the ESP atomic charges. Among the various crystal models, each differing in the size and ratio of the base-plane shape, those having longer [1, 1, 0] edges, some corre-

sponding to the present four models, exhibited an obvious structure transition. The chain sheets were quickly twisted as they were allowed to vary, showing similar behavior to that of the present observation, but they were subsequently flattened back, accompanied by a sliding movement of the chain sheets along their own faces, giving completely different crystal phases. This difference in the final structures observed in the two series of calculations may attributed to the difference in charge-fitting philosophy of the two GLYCAM parameters; in GLYCAM 04, there is no partial charge assigned to aliphatic hydrogen atoms. Obviously, the final structures proposed by the previous calculations were unrealistic, and the former GLYCAM 2000 parameter may not be appropriate to predict a condensed system of the carbohydrate. However, the results implied possible motional directions as actual structure transitions. In fact, the base-plane dimensions of the present crystal models had been adopted on the basis of the previous simulations; the crystal models of this type were observed to be the most smoothly transformed. More importantly, the twisted forms, commonly observed among our two different GLYCAM calculations and the CHARM calculation performed by Matthews et al.,[45] were indicative of the helical symmetry within the chain sheet, which could allow such a chain sheet to drive along the chain axis. In fact, a distinct difference among the cellulose crystal structures with the parallel chain arrangement is the chain staggering positions along the fiber axis, indicating that the sheet or individual chain sliding along the axis would be required during phase transitions.

Acknowledgments

Dr. Junji Sugiyama gave helpful advice on the crystal model dimensions. Dr. John W. Brady participated in discussions with his own results. Dr. R. Woods provided important suggestions about the GLYCAM parameters.

References

1. Meyer, K. H.; Misch, L. *Helv. Chim. Acta* **1937**, *20*, 232–244.
2. Sarko, A.; Muggli, R. *Macromolecules* **1974**, *7*, 486–494.
3. Gardner, K. H.; Blackwell, J. *Biopolymers* **1974**, *13*, 1975–2001.
4. Woodcoock, C.; Sarko, A. *Macromolecules* **1980**, *13*, 1183–1187.
5. Attala, R.; VanderHart, D. L. *Science* **1984**, *223*, 282–285.
6. VanderHart, D. L.; Attala, R. *Macromolecules* **1984**, *17*, 1465–1472.
7. Sugiyama, J.; Okano, T.; Yamamoto, H.; Horii, F. *Macromolecules* **1990**, *23*, 3196–3198.
8. Sugiyama, J.; Persson, P.; Chanzy, H. *Macromolecules* **1991**, *24*, 2461–2466.
9. Sugiyama, J.; Vuong, R.; Chanzy, H. *Macromolecules* **1991**, *24*, 4168–4175.
10. Finkenstadt, V. L.; Millane, R. P. *Macromolecules* **1998**, *31*, 7776–7783.
11. French, A. D.; Miller, D. P.; Aabloo, S. *Int. J. Biol. Macromol.* **1993**, *15*, 30–36.
12. Aabloo, A.; French, A. D. *Macromol. Theor. Simul.* **1994**, *3*, 185–191.
13. Aabloo, A.; French, A. D.; Mikesaar, R.; Prestin, A. J. *Cellulose* **1994**, *1*, 161–168.
14. Viëtor, R. J.; Mazeau, K.; Lakin, M.; Pérez, S. *Biopolymers* **2000**, *54*, 342–354.
15. Nishiyama, Y.; Sugiyama, J.; Chanzy, H.; Langan, P. *J. Am. Chem. Soc.* **2003**, *125*, 14300–14306.
16. Nishiyama, Y.; Langan, P.; Chanzy, H. *J. Am. Chem. Soc.* **2002**, *124*, 9074–9082.
17. Hardy, B. J.; Sarko, A. *Polymer* **1996**, *37*, 1833–1839.
18. Heiner, A. P.; Sugiyama, J.; Teleman, O. *Carbohydr. Res.* **1995**, *273*, 207–223.
19. Heiner, A. P.; Teleman, O. *Pure Appl. Chem.* **1996**, *68*, 2187–2192.
20. Heiner, A. P.; Teleman, O. *Langmuir* **1997**, *13*, 511–518.
21. Heiner, A. P.; Kuuti, L.; Teleman, O. *Carbohydr. Res.* **1998**, *306*, 205–220.
22. Mazeau, K.; Heux, L. *J. Phys. Chem. B* **2003**, *107*, 2394–2403.
23. Kroon-Batenburg, L. M. K.; Bouma, B.; Kroon, J. *Macromolecules* **1996**, *29*, 5695–5699.
24. Kroon-Batenburg, L. M. K.; Kroon, J. *Glycoconjugate J.* **1997**, *14*, 677–690.
25. Marhoefer, R. J.; Reiling, S.; Brickmann, J. *Ber. Bunsen-Ges. Phys. Chem.* **1996**, *100*, 1350–1354.
26. Reiling, S.; Brickmann, J. *Macromol. Theor. Simul.* **1995**, *4*, 725.
27. Neyertz, S.; Pizzi, A.; Merlin, A.; Maigret, B.; Brown, D.; Deglise, X. *J. Appl. Polym. Sci.* **2000**, *78*, 1939–1946.
28. Biermann, O.; Hadicke, E.; Koltzenburg, S.; Muller-Plathe, F. *Angew. Chem., Int. Ed.* **2001**, *40*, 3822–3825.
29. Mazeau, K.; Vergelati, C. *Langmuir* **2001**, *18*, 1919–1927.
30. Tanaka, F.; Fukui, N. *Cellulose* **2004**, *11*, 33–38.
31. Case, D. A.; Darden, T. A.; Cheatham, T. E., III; Simmerling, C. L.; Wang, J.; Duke, R. E.; Luo, R.; Merz, K. M.; Wang, B.; Pearlman, D. A.; Crowley, M.; Brozell, S.; Tsui, V.; Gohlke, H.; Mongan, J.; Homak, V.; Cui, G.; Beroza, P.; Schafmeister, C.; Caldwell, J. W.; Ross, W. S.; Kollman, P. AMBER 8; University of California: San Francisco, 2004.
32. Kirchner, K. N.; Woods, R. *Proc. Natl. Acad. Sci. U.S.A.* **2001**, *98*, 10541–10545.
33. Basma, M.; Sundara, S.; Calgan, D.; Venali, T.; Woods, R. *J. Comput. Chem.* **2001**, *22*, 1125–1137.
34. Kirchner, K. N.; Woods, R. J. *J. Phys. Chem. A* **2001**, *105*, 4150–4155.
35. Jorgensen, W. L.; Chandrasekhar, J.; Madura, J. D.; Impey, R. W.; Klein, M. L. *J. Phys. Chem.* **1983**, *79*, 926–935.
36. Verlet, L. *Phys. Rev.* **1967**, *159*, 98–103.
37. Ryckaert, J. P.; Cicotti, G.; Berendsen, H. J. C. *J. Comput. Phys.* **1977**, *23*, 327–341.
38. Essmann, U.; Perera, L.; Berkowitz, M. L.; Darden, T. A.; Lee, H.; Pedersen, L. G. *J. Chem. Phys.* **1995**, *103*, 8577.
39. Humphrey, W.; Dalke, A.; Schulten, K. *J. Mol. Graphics* **1996**, *14*, 33–38.

40. Bock, K.; Duus, J. Ø. *J. Carbohydr. Chem.* **1994**, *13*, 513–543.
41. Nishida, Y.; Ohrui, H.; Meguro, H. *Tetrahedron Lett.* **1984**, *24*, 1575–1578.
42. Nishida, Y.; Ohrui, H.; Meguro, H. *J. Carbohydr. Chem.* **1988**, *7*, 239.
43. Marchessault, R. H.; Pérez, S. *Biopolymers* **1979**, *28*, 2369–2374.
44. *Secondary Xylem Formation. Introduction to Biomass Science*; Fukushima, K., Funada, R., Sugiyama, J., Takabe, K., Umezawa, T., Yamamoto, H., Eds.; Kaiseisha Press, 2002; p 94.
45. Matthews, J. F.; Skopec, C. E.; Mason, P. E.; Zuccato, P.; Torget, R. W.; Sugiyama, J.; Himmel, M. E.; Brady, J. W. *Carbohydr. Res.* **2006**, *341*, 138–152.